



## PERFORMANCE OF STRUCTURAL CONCRETE FRAMES REINFORCED WITH GFRP GRID

Aly M. SAID<sup>1</sup> and Moncef L. NEHDI<sup>2</sup>

### SUMMARY

The use of fibre-reinforced polymers (FRP) rebar in structural applications has been getting increasing attention due to the advantages it offers over conventional reinforcement (e.g. durability, light weight, magnetic neutrality). A possible application of FRP rebar reinforcement is in the area of multi-storey structural frames. However, current design standards and detailing criteria for beam-column joints were established in the 1970's and may be considered unsuitable for FRP reinforcement due to its different mechanical properties. During recent earthquakes, many structural collapses were initiated or caused by beam-column joint failures. There are no comprehensive seismic standards for the application of FRP materials. Consequently, research is needed to gain a better understanding of the behaviour of FRP materials and their interaction with traditional materials in such application in order to implement their use on solid grounds. In this study, two full-scale quasi-static loading tests were performed on beam-column joint specimens. The first test was performed on a joint specimen reinforced with steel and its behaviour was compared to that of a second similar test performed on a GFRP-reinforced joint specimen. It is shown that GFRP-reinforced frames can have satisfactory drift capacity, but their energy dissipation capacity is limited.

### INTRODUCTION

Corrosion of reinforcing steel has been the primary cause of deterioration of reinforced concrete (RC) structures requiring multi-million annual repair costs around the world. According to the Technology Road Map report [1], 40% of the world production of steel is used to repair corrosion problems. Furthermore, modern equipments that employ magnetic interferometers, such as in hospitals, require a nonmagnetic environment with no metallic reinforcement. This has led to an increasing interest in FRP reinforcement, which is inherently nonmagnetic and resistant to corrosion. FRP reinforcement also provides the option of easily embedding fibre optic strain measurement devices for structural health monitoring purposes. However, FRP materials often exhibit lower ductility and weaker bond to concrete compared to that of conventional steel reinforcement. The bond of FRP to concrete can be improved by means of mechanical anchorages such as surface deformations and sand coating, but its lower ductility remains a major concern, especially in structures subjected to dynamic loading.

---

<sup>1</sup> Ph. D. Candidate, The University of Western Ontario, London, Canada.

<sup>2</sup> Associate Professor, The University of Western Ontario, London, Canada. Email: mnehdi@eng.uwo.ca.

Brown and Bartholomew [2] observed that FRP-reinforced beams behaved in a similar manner to that of steel-reinforced beams. They argued that strength design methods for steel-reinforced beams can predict the ultimate moment capacity of FRP-reinforced beams. However, in the design process, two criteria that are not usually a major concern in the case of steel reinforcement can govern the design in the case of FRP reinforcement: deflection and ductility. FRP rebars usually have a significantly lower modulus of elasticity compared to that of steel rebars and thus, often generate higher deflections. Furthermore, the predominantly elastic behaviour of FRP rebars results in little warning before a usually sudden and brittle failure. Therefore, satisfying deflection and ductility requirements are a challenge in designing FRP-reinforced concrete structures.

Recently, there has been an increasing interest to investigate steel-free FRP-reinforced concrete structures. However, research in this area has been generally limited to some beam and column testing under monotonic loading. Most of the newly adopted specifications for the design of FRP-reinforced concrete [3-7] are not comprehensive and often do not include detailed seismic provisions. Therefore, research is needed to investigate the performance of steel-free FRP-reinforced concrete frames under quasi-static loading in order to form the basis for future design code provisions for FRP-reinforced concrete in seismic zones. In this study, full-scale steel-reinforced and steel-free GFRP-reinforced beam-column joints were tested under quasi-static loading and their behaviour including load-storey drift envelope relationship and energy dissipation were compared and discussed.

### **SCOPE OF PREVIOUS WORK**

The use of FRP reinforcement in various structural elements has been widely investigated. Work on RC beams covers different permutations of FRP and steel as longitudinal and transverse reinforcement, respectively [8-10]. However, reinforcing steel in RC elements is vulnerable to corrosion, especially the transverse reinforcement for which the concrete cover is thinner. The use of FRP stirrups has been hindered by their limited availability. Moreover, a 60% strength reduction factor at bends for various types of FRP is recommended [5], which makes them less appealing. Also, bending FRP bars to make stirrups has to be performed in production plants with special care and equipment. The use of FRP NEFMAC grids can provide a solution to such a problem; a four-cell unit taken from a grid provides a three-branched stirrup.

Fibre-reinforced polymers were also used in slabs in the form of composite grids for instance by Bantia *et al.* [11] (CFRP), Rahman *et al.* [12] (CFRP), and Yost and Schmeckpeper [13] (hybrid GFRP-CFRP). The general conclusion was that FRP grids are a suitable material for reinforcing concrete slabs and that the punching shear strength is lower than that of similar steel-reinforced slabs [14]. Also, studies recommended that flexural design of FRP-reinforced slabs and beams should aim at an over-reinforced section in order to achieve a compression failure [15]. This recommendation was also adopted by design codes such as ACI 440.1R-01 [6] because a compression failure usually allows FRP-reinforced flexure members to exhibit some plastic behaviour before failure.

Girra and Saatcioglu [16] investigated the use of both steel and CFRP grids as stirrups for confinement of columns with longitudinal steel reinforcement. Several configurations of transverse reinforcement were tested under cyclic loading. They concluded that the performance of columns reinforced with CFRP stirrups was comparable to that of columns reinforced with steel stirrups. They also argued that the use of grids in general, beside ease of construction, provided a near-uniform distribution of the confinement pressure along the column, without congesting the reinforcement cage. They reported that the NEFMAC grid-based stirrups failed at the nodes, which is the common weakness of FRP stirrups.

Fukuyama *et al.* [17] tested a half-scale three-storey AFRP-reinforced concrete frame under quasi-static loading. RA11S aramid-bars were used for the main columns reinforcement, RA7S bars were used as flexural reinforcement for beams and slabs, while RA5 bars were used as shear reinforcement. RA11S, RA7S and RA5 are braided bars with cross-sectional areas of 90, 45 and 23 mm<sup>2</sup>, respectively. It was argued that frame deformations would govern the design. The frame remained elastic up to a drift angle of 1/50 rad, and no substantial decrease in strength took place after rupture of some main beam rebars owing to the high degree of indeterminacy of the frame. It was also noted that the rehabilitation of such a frame was easier than that of conventional RC frames since residual deformations were smaller. However, the frame was not tested up to failure and its behaviour under excessive deformations was not reported. Thus, testing a steel-free FRP-reinforced standard frame up to failure should provide valuable information.

## ADVANTAGES OF USING FRP GRIDS

Unidirectional FRP grid-reinforced concrete structures provide a wide range of possible applications. These include concrete bridge decks, barrier walls, water tanks, slabs-on-grade, curtain walls, underground tunnel linings, rock storage cavities, etc. [18]. The advantages of FRP grids include suppression of delamination problems, equal longitudinal and transverse reinforcement depth, built-in redundancy [19], and high durability and fatigue resistance [12]. In general, the grid structure being lightweight and manufactured into either curved or flat plates, drastically reduces assembly work at construction sites. Offsite construction also allows for better quality control and assurance. Because of its corrosion resistance, FRP grids constitute a promising technology for reinforcing concrete structures in offshore and coastal regions and in environments where corrosive de-icing salts are used. Furthermore, the magnetic neutrality characteristic of FRP makes it an ideal reinforcing material for instance in structures housing hospitals where magnetic resonance imaging (MRI) equipment is in common use.

The type of FRP used in this study is NEFMAC (*New Fiber Composite Material for Reinforcing Concrete*). NEFMAC can be made from glass, aramid, or carbon fibres (or a hybrid combination) in a batch process. The fibres are impregnated with a resin (polyester, vinylester or epoxy). Using a layering process, individual FRP laminates are formed into rigid 2D rectangular grid shapes. The longitudinal and transverse bars are orthogonal and continuous at the intersection points so that there is a 2D symmetry of mechanical and geometric properties. Bars have a rectangular cross-section, with smooth top and bottom surfaces and rough fibrous sides.

## EXPERIMENTAL PROGRAM

Beam-column joints can be isolated from plane frames at the points of contraflexure. The beam of the current test unit is taken to the mid-span of the bay, while the column is taken from the mid-height of one storey to the mid-height of the next storey.

### Steel-Reinforced Specimen (*J1*)

The first specimen constructed in this study is a standard beam-column joint (*J1*) designed to satisfy both CSA A23.3-94 [20] and ACI 352R-02 [21] requirements. It has sufficient shear reinforcement in the joint area, in the column hinging area, and in the beam hinging area. Dimensions and reinforcement details for the standard specimen (*J1*) are shown Fig. 1 (a).

### GFRP-Reinforced Specimen (*J4*)

The second beam-column joint specimen constructed in this study (*J4*), shown in Fig. 1(b), had identical dimensions to specimen (*J1*) but was made with GFRP grid reinforcement and a different reinforcement configuration. A view of the GFRP reinforcement cage is shown in Fig. 2. The longitudinal GFRP rebars used were NEFMAC G16 (201 mm<sup>2</sup> of cross-sectional area) with 5 nodes per meter in the beam, but this

was increased to 10 nodes per meter in the joint area for extra mechanical anchorage and to avoid premature slippage of the beam reinforcement from the joint. The rebars used in the column had 5 nodes per meter. All GFRP longitudinal rebars had nodes 50 mm wide from end to end. The longitudinal reinforcement configuration aimed at providing a similar bending moment capacity to that of the standard steel-reinforced specimen, thus inducing a comparable level of joint shear input. The transverse reinforcement in specimen (*J4*) consisted of 3-branched (vertically and horizontally) G10 (77 mm<sup>2</sup> of cross-sectional area) stirrups. This provides built in redundancy since the failure of a branch is not complete until both of its two vertical portions fail. Some properties of the NEFMAC grids are listed in Table 1. GFRP was chosen instead of CFRP since its strain at failure is 67% higher, which should give a better indication of imminent failure owing to larger ultimate deformations.

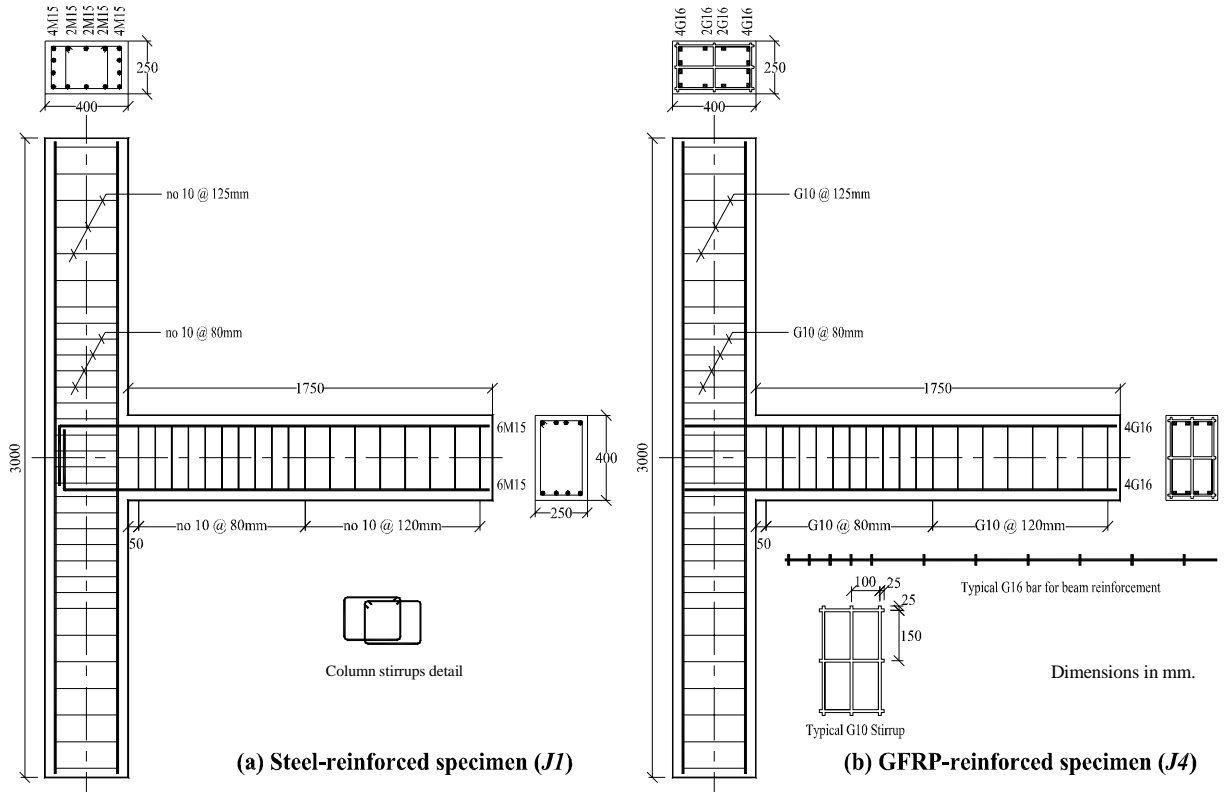


**Fig. 1. Reinforcement details and strain gauges' locations for (a) the steel-reinforced specimen (*J1*), and (b) the GFRP-reinforced specimen (*J4*).**

**Table 1. Properties of NEFMAC grids [22]**

Bar No.	Sectional Area (mm <sup>2</sup> )	Max Load (kN)	Tensile Strength (MPa)	Modulus of Elasticity (MPa)
G10	77	46.7	600	30
G16	201	119.2	600	30

The assembly of the GFRP-reinforced specimen (*J4*) was performed at a much faster pace than that of the steel-reinforced specimen (*J1*). The stirrups, being taken from a manufactured grid, were dimensionally identical. Accordingly, the longitudinal reinforcement needed very little rearrangement. The much lighter weight of the GFRP rebars allowed easier manipulation of the reinforcement cage. For the steel-reinforced specimen (*J1*), extra work was required to fit steel rebars in place, especially in the joint area. The

congestion of the joint area with steel reinforcement and the difficulty of casting concrete in it prompted a part of the research program to focus on studying the usage of self-consolidating concrete [23].



**Fig. 2. View of the GFRP reinforcement cage for specimen (J4) lifted on the forms before casting.**

### **Test Setup and Procedure**

The beam-column joint specimens were tested under a constant axial load of 600 kN applied on the column and reversed cyclic load (quasi-static) applied at the beam tip. The selected loading pattern applied at the beam tip was intended to cause forces that induce high levels of deformations usually experienced by structural frames during severe earthquakes.

For the steel-reinforced specimen, the selected load history consisted of two phases. The first one was load-controlled in which two load cycles at approximately 10% of the estimated strength of the specimen were applied to check the test setup. This was followed by two load cycles reaching the concrete flexural cracking load in the beam at the column face. These in turn were followed by two cycles at the load causing initial yield in the beam. The displacement at initial yield of the beam section adjacent to the column face,  $\delta_y$ , was recorded and used in the subsequent displacement-controlled phase of loading. In this second displacement-controlled phase, multiples of the yield displacement,  $\delta_y$ , were applied to the specimen. For each load increment, two consecutive cycles were applied at the same loading level to verify the stability of the specimen.

A different loading routine was selected for the GFRP-reinforced specimen (J4) since unlike conventional steel-reinforced sections, those reinforced with GFRP do not undergo yielding. A displacement-controlled load history similar to the one used by Fukuyama *et al.* [17] was applied in which incremental values of drift were imposed on the specimen. Drift was applied starting at 1/2000 rad, then increased at pre-specified values (1/1000, 1/800, ....., 1/33, 1/22, 1/20 rad) in both directions as shown in Fig. 3. The very first drift was applied in one cycle, while all other subsequent drifts were applied in two cycles. Further details about test setup are available elsewhere [23].

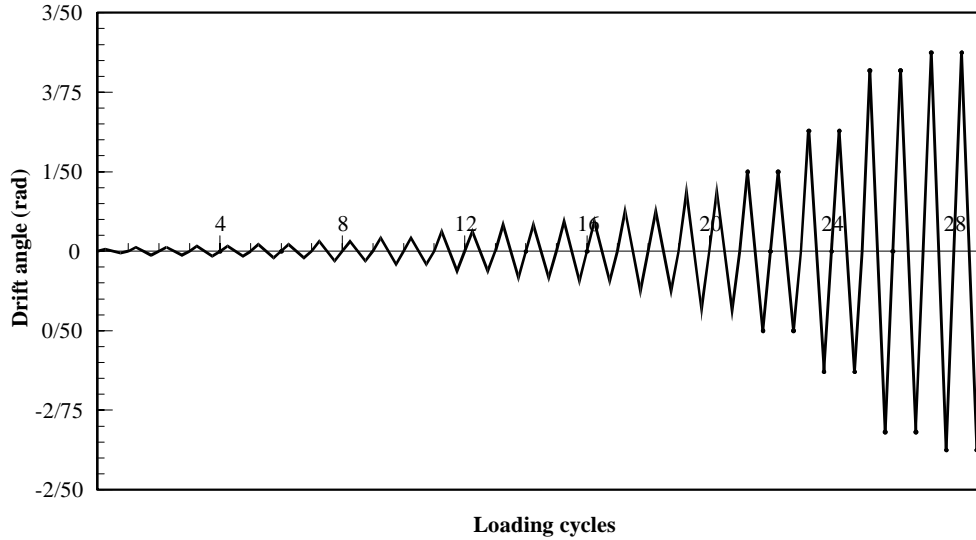


**Fig. 3. Load history for the reversed cyclic load test used for the GFRP-reinforced specimen (J4).**

### ANALYSIS OF TEST RESULTS

#### Behaviour of Steel-Reinforced Specimen (J1)

The load-displacement plot for the standard specimen is shown in Fig. 4. First flexural cracking of the beam section subjected to maximum bending moment appeared at a beam tip load of 15 kN corresponding to a drift of 0.0017 rad. The onset of diagonal cracks in the joint area took place at a beam tip load of 50 kN corresponding to a drift of 0.006 rad.

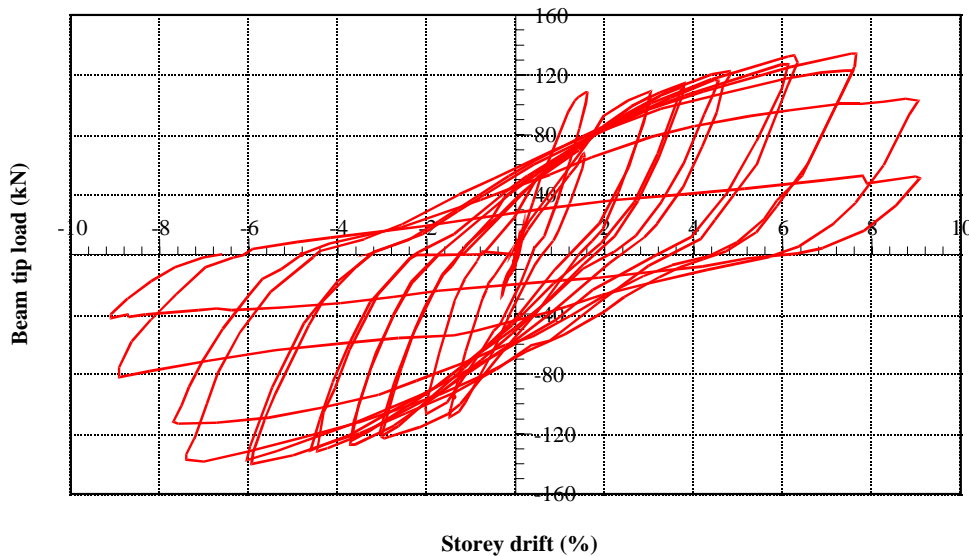


**Fig. 4. Beam tip load-storey drift relationship for the standard steel-reinforced specimen (J1).**

Additional cracks in the joint area appeared thereafter as loading progressed, but remained within a very fine width throughout the test. The yield of the beam's longitudinal steel was reached at an average beam tip load of 107 kN and the corresponding average yield displacement,  $\delta_y$ , was 28 mm (corresponding to a drift of 0.0150 rad, based on the average of push up and pull down values). At a deformation level equal to  $2\delta_y$ , the beam became extensively cracked along a distance equal to its depth from the face of the

column. At a deformation equal to  $4\delta_j$ , wide cracks developed in the hinge area of the beam and rubble started falling. At  $6\delta_j$ , the flexural hinge area of the beam lost most of its concrete. The test was stopped as the beam capacity dropped but the axial load in the column was maintained and the joint areas remained still intact, except the presence of fine cracks. The final crack pattern of the standard specimen (*J1*) is shown in Fig. 5 (a). After the test termination, two longitudinal rebars (one top and one bottom) were detected failing in tension.

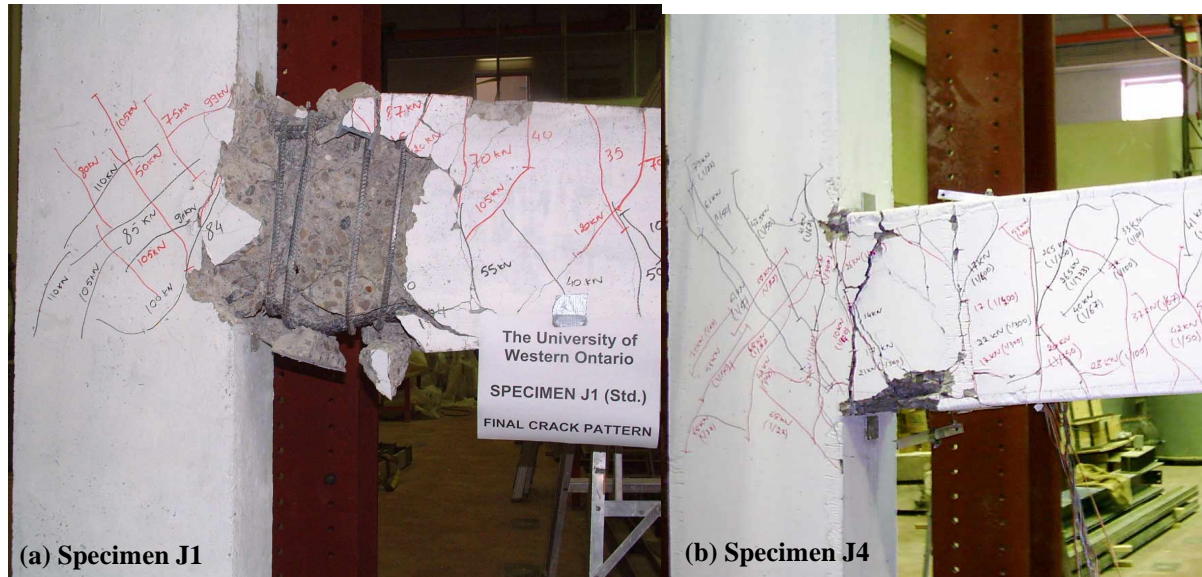


**Fig. 5. Final crack pattern for (a) the steel-reinforced specimen (*J1*), and (b) the GFRP-reinforced specimen (*J4*).**

#### **Behaviour of GFRP-Reinforced Specimen (*J4*)**

The load-displacement plot for the GFRP-reinforced specimen is shown in Fig. 6. The first flexural crack at the beam bottom adjacent to the column face was detected at a drift angle of  $1/1000$  rad corresponding to a beam tip load of about 10.5 kN. A permanent beam-tip deformation of 1.6 mm was measured after the  $1/400$  rad drift cycles. As the test progressed, several distinct cracks extended through the depth of the beam section at specific locations corresponding to grid nodes in the longitudinal reinforcement, while several smaller cracks formed along the beam. This took place since bars, which are originally cut from grids, are not deformed and the bond with concrete is predominantly supplied by the nodes. The onset of diagonal cracks in the joint area took place at a beam tip load of 42 kN during the  $1/50$  rad drift cycle. Additional cracks in the joint area appeared thereafter as loading progressed, but remained within a very fine width throughout the test. At a drift angle of  $1/22$  rad, the beam became excessively cracked and rubble started falling. Failure took place at the  $1/20$  rad drift angle in a sudden and brittle manner when two of the beam's bottom GFRP bars snapped in tension. The final crack pattern of the GFRP-reinforced specimen (*J4*) is shown in Fig. 5 (b).

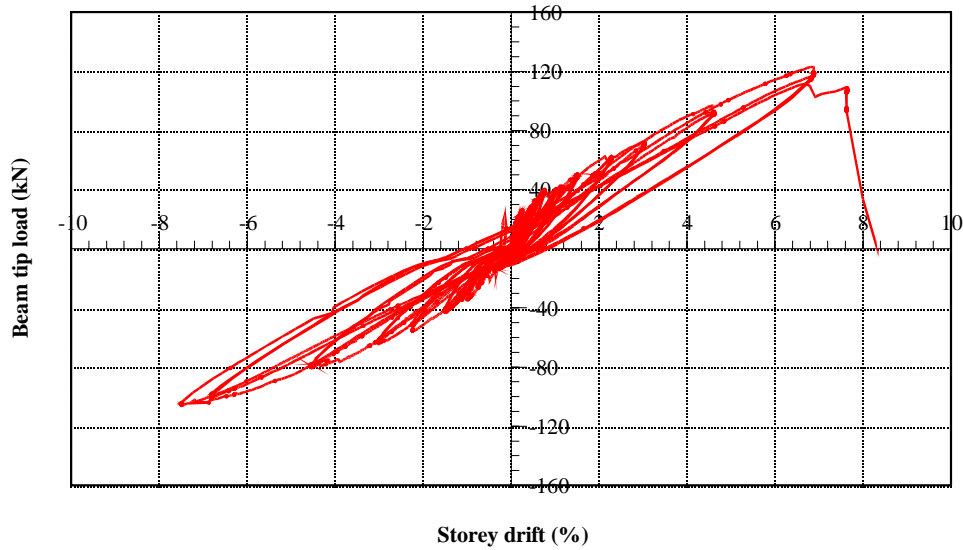


Fig. 6. Beam tip load-storey drift relationship for the GFRP-reinforced specimen (*J4*).

#### Load – Storey Drift Angle Envelope Relationship

For the tested beam-column joint specimens, the envelope of the beam tip load-storey drift angle relationships are shown in Fig. 7. Comparing the two envelopes shows a lower load capacity and stiffness for the GFRP-reinforced specimen, which is due to the lower stiffness of GFRP compared to that of steel. The envelopes started at comparable stiffness, but as soon as cracking took place a distinct difference between the two appeared and was significant for the remainder of the tests. The steel-reinforced specimen (*J1*) had about 23% higher total drift at the end of the test compared to that of the GFRP-reinforced specimen and did not exhibit sudden loss of strength. The GFRP-reinforced specimen (*J4*) had an essentially elastic envelope, whereas the steel-reinforced specimen (*J1*) had a typical elastic-plastic envelope.

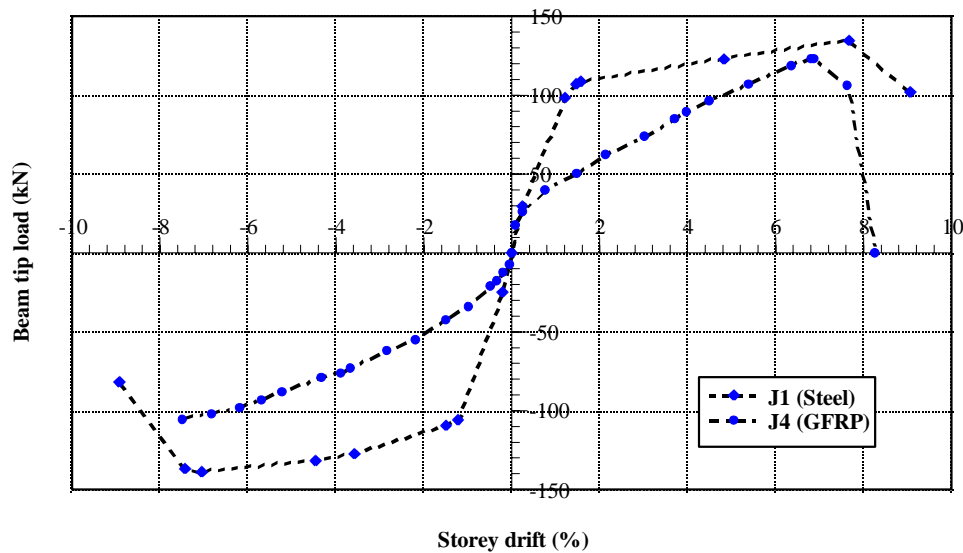
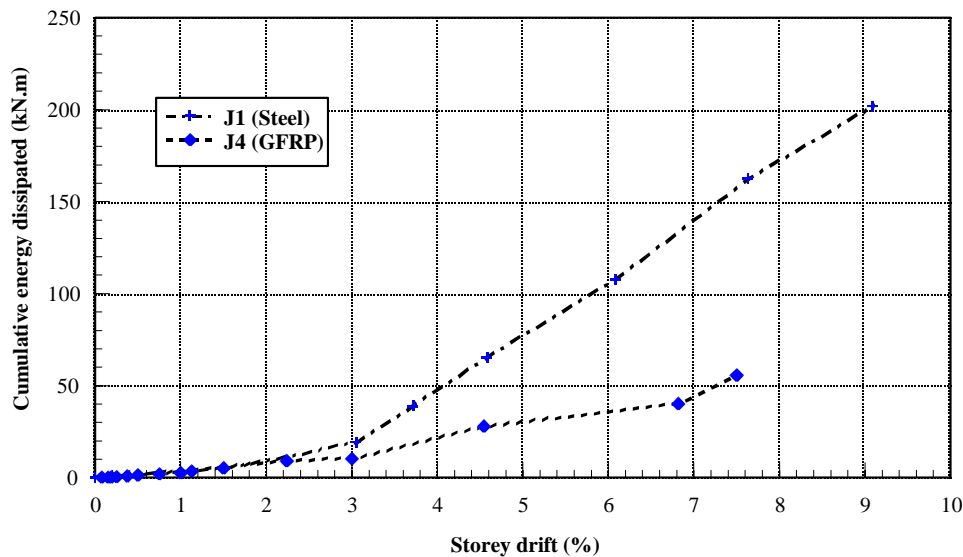


Fig. 7. Beam tip load-storey drift envelopes for the tested specimens.

### Cumulative Dissipated Energy

The capability of a structure to survive an earthquake depends on its ability to dissipate the energy input from ground motion. Although it is difficult to estimate such an energy input during a ground movement event, a satisfactory design should ensure a larger energy dissipation capability of the structure than the demand. The cumulative energy dissipated by the beam-column joint specimens during the reversed cyclic load tests was calculated by summing up the energy dissipated in consecutive load-displacement loops throughout the test. The energy dissipated in a cycle is calculated as the area that the hysteretic loop encloses in the corresponding beam tip load-displacement plot. Fig. 8 shows plots of the cumulative energy dissipation versus storey drift for the tested specimens. Results displayed in Fig. 8 show that the GFRP-reinforced specimen (*J4*) had about 25% of the energy dissipation capacity of the standard steel-reinforced specimen (*J1*) before failure. This is clear from the shape of individual hysteretic loops of the tested specimens (Figs. 4 and 6) which are much wider for the steel-reinforced specimen. The ductility of steel reinforcement allowed higher plastic deformations to occur in the beam, thus increasing the area of each individual loop. The damage levels that the specimens sustained at failure, shown in Fig. 5, indicate that while for the steel-reinforced specimen extensive cracking in the beam hinge area helped the specimen to dissipate energy, the GFRP-reinforced specimen sustained severe but localized damage. Yielding of steel is a major mechanism for RC structures to dissipate energy, whereas plastic deformations and friction along cracks in concrete usually have lower contribution to the total energy dissipated.



**Fig. 8. Cumulative energy dissipated for the tested specimens.**

### Storey Shear - Joint Shear Deformation Relationship

The beam-column joint stiffness was monitored through the measurement of the joint panel deformation obtained using two LVDT's mounted diagonally across the corners of the joint area. The measured elongation and shortening of the joint diagonals versus load was used to derive the average joint shear deformation, which is equal to the sum of the horizontal and vertical shear deformation angles, denoted as  $\gamma_h$  and  $\gamma_v$ , respectively. The average shear deformation,  $\gamma_{average}$ , can be calculated as:

$$\gamma_{average} = \gamma_h + \gamma_v = \frac{\Delta_1 + \Delta_2}{D \sin 2\Phi}$$

Where  $\Delta_1$  and  $\Delta_2$  are the elongation and shortening in the lengths of the diagonals, respectively,  $D$  is the length of the diagonal and  $\Phi$  is the angle between the diagonal and the axis of the beam.

The storey shear-joint deformation plots for specimens *J1* and *J4* are traced in Fig. 9, on similar horizontal scale. The storey shear,  $V_{actual}$ , was calculated taking into account the  $P-\Delta$  effect based on work of Uzumeri and Seckin [24] using the following equation:

$$V_{actual} = \frac{P\left(L/2 - \frac{\delta}{L/2}H\right) - N \times \frac{\delta}{L/2}H}{H}$$

Where  $N$  is the column axial load,  $H$  is the column height,  $L$  is the beam's length, and  $P$  and  $\delta$  are the beam tip load and deformation, respectively.

Comparing the behaviour of both joint panels, it is clear that the steel-reinforced panel of specimen (*J1*) had higher stiffness and smaller joint deformation compared to that of the GFRP-reinforced panel. This produced higher joint contribution to the total deformation of the subassembly in the case of the GFRP-reinforced specimen (*J4*), which normally adds up to the lateral deformation of the frame. Fukuyama *et al.* [17] noticed that the measured lateral deformations for the 2 bay-3 storey half-scale frame that they tested exceeded the calculated values, which was attributed to joint panel deformations. However, since no joint panel deformation measurements were made in their test, this assumption which was not fully confirmed in their study is apparent in the results of the current study.

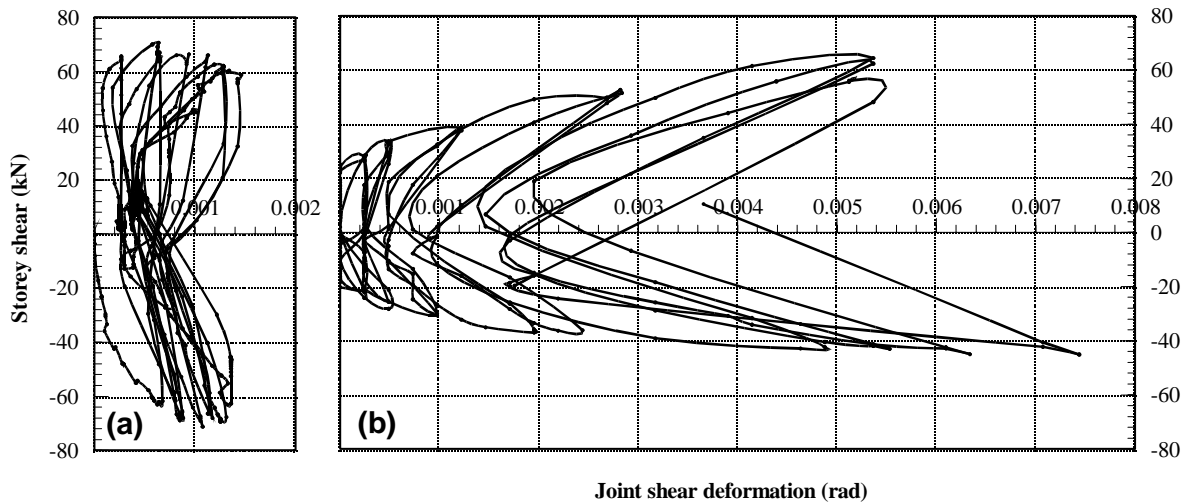


**Fig. 9. Variation of the storey shear versus joint shear deformation for the (a) steel-reinforced specimen (*J1*) and (b) GFRP-reinforced specimen (*J4*).**

## CONCLUSIONS

An experimental investigation was performed to study the behaviour of beam-column joints reinforced using GFRP rebar and GFRP stirrups and compare it to that of standard steel-reinforced beam-column joints under quasi-static loading. Based on experimental observations and analysis of test results, the following conclusions can be drawn:

1. The GFRP-reinforced beam-column joint showed a predominantly elastic behaviour with very low plasticity features when tested under quasi-static loading. This resulted in lower energy dissipation compared to that of the conventional steel-reinforced beam-column joint.
2. The GFRP-reinforced beam-column joint showed lower stiffness than that of the conventional steel-reinforced beam-column joint.

3. The GFRP-reinforced specimen showed a satisfactory drift capacity, assuming a minimum drift requirement of 3% as recommended in the literature for ductile frame buildings [25]. However, the standard specimen still outperformed the GFRP-reinforced specimen.
4. In view of the observed ductility limitations of steel-free GFRP-reinforced structural frames under quasi-static loading, a designer may explore using hybrid systems in which steel-reinforced structural members provide lateral load resistance, while GFRP-reinforced members are used in the envelope of the structure, thus inhibiting corrosion and other durability problems.
5. This study was only focussed on the level of the subassemblage. A more global concept should be adopted in the design of moment-resisting frames. Thorough dynamic analysis of GFRP-reinforced structures should be performed to better assess their capacity in meeting seismic resistance requirements.
6. Design code provisions for the seismic design of RC structures which have been developed for ductile steel reinforcement need to be re-evaluated for FRP-reinforced structures to address their low energy dissipation capacity.

## REFERENCES

1. Canadian Society of Civil Engineering (2003). "Civil Infrastructure Systems-Technology Road Map 2003-2013", CSCE, [http://www.csce.ca/TRM/TRM-Report\\_english\\_01.pdf](http://www.csce.ca/TRM/TRM-Report_english_01.pdf).
2. Brown, V. L. and Bartholomew, C. L. (1993). "FRP Reinforcing Bars in Reinforced Concrete Members", *ACI Mat. J.*, 90 (1), 34-39.
3. Japanese Society of Civil Engineers, JSCE (1997). "Recommendations for the Design and Construction of Concrete Structures Using Continuous Fiber Reinforcing Materials", *Concrete Engineering Series 23*, Edited by A. Machida.
4. Canadian Highway Bridge Design Code (CHBDC). (1998). "Fibre Reinforced Structures", Section 16, 687-705.
5. ISIS Canada Manual No. 3 (2001). "Reinforcing Concrete Structures with Fibre Reinforced Polymers", S. Rizkalla and A. Mufti (Authors).
6. ACI 440.1R-01 (2001). "Guide for the Design and Construction of Concrete Reinforced with FRP Bars", ACI Committee 440 Report.
7. CSA S806-02 (2002). "Design and Construction of Building Components Using Fibre-Reinforced Polymers", Canadian Standards Association, Rexdale, Ontario, Canada.
8. Nagasaka, T., Fukuyama, H. and Tanigaki, M. (1993). "Shear Performance of Concrete Beams Reinforced with FRP Stirrups", *ACI, SP-138*, A. Nanni and C. Dolan (Editors), 789-811.
9. Alsayed, S. H., Al-Salloum, Y. A. and Almusallam, T. H. (1997). "Shear Design of GFRP Bars", *Proc. 3rd Int. Sym. on Non-Metallic (FRP) Reinforcement for Concrete Structures, FRPRCS-3*, Sapporo, Japan, Vol. 2, 285-292.
10. Shehata, E. F. G. (1999). "Fibre-Reinforced Polymer (FRP) for Shear Reinforcement in Concrete Structures", Ph. D. Thesis, University of Manitoba, Winnipeg, Manitoba, Canada.
11. Bantia, N., Al-Asaly, M. and Ma, S. (1995). "Behavior of Concrete Slabs Reinforced with Fiber-Reinforced Plastic Grid", *J. Mat. in Civ. Engrg., ASCE*, 7 (4), 252-257.
12. Rahman, A. H., Kingsley, C. Y. and Kobayashi, K. (2000). "Service and Ultimate Load Behavior of Bridge Deck Reinforced with Carbon FRP Grid", *J. Comp. for Const., ASCE*, 4 (1), 16-23.
13. Yost, J. R. and Schmeckpeper, E. R. (2001). "Strength and Serviceability of FRP Grid Reinforced Bridge Decks", *J. Bridge Engrg., ASCE*, 6 (6), 605-612.
14. Matthys, S. and Taerwe, L. (2000). "Concrete Slabs Reinforced with FRP Grids. II: Punching Resistance", *J. Comp. for Const., ASCE*, 4 (3), 154-161.
15. Nanni, A. (1993). "Flexural Behavior and Design of RC Members Using FRP Reinforcement", *J. Struct. Engrg., ASCE*, 119 (11), 3344-3359.

16. Grira, M. and Saatcioglu, M. (1999). "Reinforced Concrete Columns Confined with Steel or FRP Grids", Proc. of the 8th Canadian Conf. on Earthquake Engineering, Vancouver, Canada, 445-450.
17. Fukuyama, H., Masuada, H., Sonobe, Y., and Tanigaki, M. (1995). "Structural Performance of Concrete Frames Reinforced with FRP Reinforcement", Proc. of the 2nd Int. RILEM Sym. on Non-Metallic (FRP) Reinforcement for Structures, FRPRCS-2, Ghent, Belgium, 275-286.
18. Sugita, M. (1993). "NEFMAC Grid Type Reinforcement", A contribution to Alternative Materials for The Reinforcing and Prestressing of Concrete, edited by Clarke, J. L., Blackie Academic and Professional, UK, 55-82.
19. Dutta, P. K., Bailey, D. M., Tsai, S. W., Jensen, D. W., Hayes Jr., J. R., McDonald, W. E., Smart, C. W., Colwell, T., Earl, J. S. and Chen, H. -J. (1998). "Composite Grids for Reinforcement of Concrete Structures", US Army Corps of Engineers, Construction Engineering Research Laboratories, USACERL Technical Report 98/81.
20. CSA A23.3-94 (1994). "Design of Concrete Structures", Canadian Standards Association, Rexdale, Ontario, Canada.
21. ACI 352R-02 (2002). "Recommendations for Design of Beam Column Connections in Monolithic Reinforced Concrete Structures", Joint ACI-ASCE Committee 352, Technical Committee Document 352R-02.
22. NEFCOM Corporation (1996). "Mechanical Properties of NEFMAC", Tokyo.
23. Said, A. and Nehdi, M. (2004). "The Use of Self-Compacting Concrete in Moment Resisting Frames in Seismic Regions", Proceedings of the 13<sup>th</sup> World Conference on Earthquake Engineering, Paper No. 1686.
24. Uzumeri, S. M. and Seckin, M. (1974). "Behaviour of Reinforced Concrete Beam-Column Joints Subjected to Slow Load Reversals", Report No. 74-05, Department of Civil Engineering, University of Toronto, Toronto, Ontario, Canada.
25. Corley, W. G. (1995). "Ductility of Column, Wall, and Beams-How Much is Enough?", Proc. of The Thomas Paulay Sym., Recent Developments in Lateral Force Transfer in Buildings, ACI, SP-157, Sept. 20-22, 1993, La Jolla, California, 331-350.